

## Chapter I

# Introduction

### 1.1 | A tour of the fluvial system

The fluvial system is classically divided into erosional, transportational, and depositional regimes (Schumm, 1977). In the Basin and Range province of the western US, Cenozoic tectonic extension has produced a semi-periodic topography with high ranges (dominated by erosion) and low valleys (dominated by deposition). In this region, all three fluvial-system regimes can be found within distances of 10–20 km. As an introduction to the scientific questions addressed in this book, we start with a tour of the process zones of the fluvial system, using Hanau-pah Canyon, Death Valley, California, as a type example (Figure 1.1).

#### 1.1.1 Large-scale topography of the basin and range province

The large-scale geomorphology of the Basin and Range is a consequence of the geometry of faults that develop during extension and the subsequent isostatic adjustment of each crustal block. In the late Cretaceous, the Basin and Range was an extensive high-elevation plateau, broadly similar to the Altiplano-Eastern Cordillera of the central Andes today. When subduction of the Farallon plate ceased beneath the western US, this region became a predominantly strike-slip plate boundary and the horizontal compressive force that supported the high topography and over-thickened crust of the region could no longer withstand the weight of the overlying topography. The result was regional extension (Sonder

and Jones, 1999). The structural style of extensional faulting varies greatly from place to place in the western US, but Figure 1.2 illustrates one simple model of extension that can help us understand the topography of the modern Basin and Range. The weight of the high topography in the region created a vertical compressive force on the lower crust. That compressive force was accompanied by an extensional force in the horizontal direction. Mechanically, all rocks respond to a compressive force in one direction with an extensional force in the other direction in order to preserve volume. This combination of compressive vertical forces and extensional horizontal forces created faults at angles of  $\approx 5\text{--}30^\circ$  to the horizontal (with smaller angles at greater depths).

Crustal blocks float on the mantle, with the weight of the crust block supported by the buoyancy force that results from the bottom of the crustal block displacing higher-density mantle rock. The shape of each crustal block partially determines how high above Earth's surface the block will stand. Normal faulting creates a series of trapezoidal crustal blocks that, while mechanically coupled by faults, can also rise and fall according to their shape. A crustal block with a wide bottom displaces a relatively large volume of high-density mantle. The resulting buoyancy requires that the block stand higher above Earth's geoid in order to be in isostatic equilibrium. Conversely, a crustal block with a relatively narrow bottom will displace a smaller volume of mantle and will hence stand lower relative to the geoid. This kind of adjustment is the fundamental



**Fig 1.1** Hanaupah Canyon and its alluvial fan, Death Valley, California.

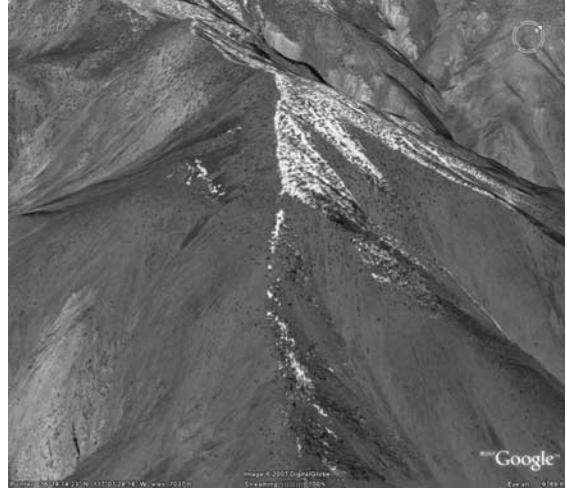


**Fig 1.3** Oblique perspective image of the high peaks of Hanaupah Canyon. Reproduced with permission of DigitalGlobe.

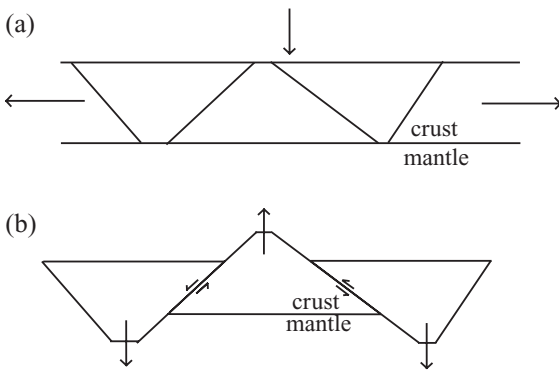


**Fig 1.2** Schematic diagram of a simple model for Basin and Range extension and isostatic adjustment. In (a), horizontal extension and vertical compression cause the creation of trapezoidal crustal blocks bounded by a series of normal faults. Crustal blocks with wide bottoms (ranges) rise to maintain isostatic balance, while blocks with narrow bottoms (basins) fall relative to Earth's geoid.

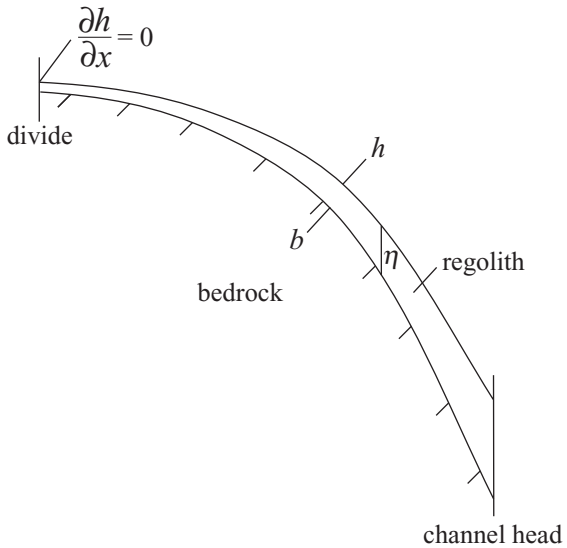


**Fig 1.4** Schematic diagram of a hillslope profile from divide to channel head.

reason why extension causes the semi-periodic topography of the Basin and Range Province.

### 1.1.2 The hillslope system

Hillslopes in the high elevations of Hanaupah Canyon are characterized by steep, planar topographic profiles and abrupt, knife-edge divides (Figure 1.3). West of the divide, water and sediment drains towards Panamint Valley, while on the east side they drain towards Death Valley. If we quantify the flux of water and sediment along a profile that includes the drainage divide, the flux of water and sediment must be negative on one side of the divide and positive on the other

because of this change in drainage direction. At the divide itself, the water and sediment flux is zero, since this is the transition point from western drainage to eastern drainage. Sediment flux on hillslopes is directly related to the topographic gradient. Therefore, since the sediment flux is zero, the topographic gradient,  $\partial h/\partial x$ , must also be zero (Figure 1.4).

Hillslopes in bedrock-dominated landscapes are composed of a system of two interacting surfaces: the topographic surface, with elevations given by  $h(x, y)$ , and the underlying weathering front, given by  $b(x, y)$  (Figure 1.4). The difference between these two surfaces is the regolith depth,  $\eta(x, y)$ . The topographic and weathering-front surfaces are strongly coupled because the shape of the topography controls erosion and deposition, which, in turn, changes the values of  $\eta(x, y)$  (Furbish and Fagherazzi, 2001). The values of  $\eta(x, y)$ , in turn, control weathering rates. The simplest system of equations that describes this feedback relationship is given by:

$$\frac{\partial \eta}{\partial t} = -\frac{\rho_b}{\rho_s} \frac{\partial b}{\partial t} - \kappa \frac{\partial^2 h}{\partial x^2} \quad (1.1)$$

and

$$\frac{\partial b}{\partial t} = -P_0 e^{-\eta/\eta_0} \quad (1.2)$$

where  $t$  is time,  $\rho_b$  is the bedrock density,  $\rho_s$  is the sediment density,  $\kappa$  is the hillslope diffusivity,  $x$  is the distance along the hillslope profile,  $P_0$  is the regolith-production rate for bare bedrock, and  $\eta_0$  is a characteristic regolith depth. Equation (1.1) states that the rate of change of regolith thickness with time is the difference between a “source” term equal to the rate of bedrock lowering multiplied by the ratio of bedrock to sediment density, and a “sink” term equal to the curvature of the topographic profile. This curvature-based erosion model is the classic diffusion model of hillslopes, first proposed by Culling (1960). The diffusion model of hillslope evolution, discussed in Chapter 2, is a consequence of conservation of mass along hillslope profiles, and the fact that sediment flux is proportional to topographic gradient if certain conditions are met. The diffusion model of hillslope evolution does not apply to the steep hillslopes of Hanaupah Canyon, however. In steep landscapes, sediment flux increases nonlinearly with the topographic gradient as the angle of stability is approached and landsliding becomes the predominant mode of sediment transport. The effects of mass movements on hillslope evolution can be captured in a nonlinear hillslope diffusion model that will also be discussed in Chapter 2. The steep, planar hillslopes and abrupt,

knife-edge drainage divides of Hanaupah Canyon are a signature of landslide-dominated, nonlinear transport on hillslopes (Roering *et al.*, 1999).

Equation (1.2) states that bedrock lowering is a maximum for bare bedrock slopes and decreases exponentially with increasing regolith thickness. This relationship has been inferred from cosmogenic isotope analyses on hillslopes (Heimsath *et al.*, 1997). Conceptually, the inverse relationship between weathering/regolith-production rate and regolith thickness is a consequence of the fact that regolith acts as a buffer for the underlying bedrock, protecting it from diurnal temperature changes and infiltrating runoff that act as drivers for physical and chemical weathering in the subsurface. In Figure 1.4, the weathering front is shown as an abrupt transition from bedrock to regolith, but in nature this boundary is usually gradual.

Equations (1.1) and (1.2) can be solved for the steady-state case in which regolith thickness is independent of time at all points along the hillslope profile:

$$\eta = \eta_0 \ln \left( \frac{\rho_b P_0}{\rho_s \kappa} \frac{1}{-\frac{\partial^2 h}{\partial x^2}} \right) \quad (1.3)$$

Equation (1.3) implies that, in steady state, regolith thickness decreases as the negative (downward) curvature increases, becoming zero (i.e. bare bedrock) where the curvature reaches a critical value of

$$\left. \frac{\partial^2 h}{\partial x^2} \right|_{bare} = -\frac{\rho_b P_0}{\rho_s \kappa} \quad (1.4)$$

Equation (1.2) is not universally applicable. As regolith thickness decreases below a critical value in arid regions, for example, the landscape is unable to store enough water to support significant plant life. Plants act as weathering agents (e.g. root growth can fracture rock, canopy cover can decrease evaporation, etc.). Therefore, in some arid environments weathering rates actually *increase* as regolith thickness increases, rather than decreasing with thickness as the exponential term in Eq. (1.2) predicts (Figure 1.5). Using a vegetation-limited model of weathering in landscape evolution models results in landscapes with a bimodal distribution of slopes (i.e. cliffs and talus slopes) similar to many

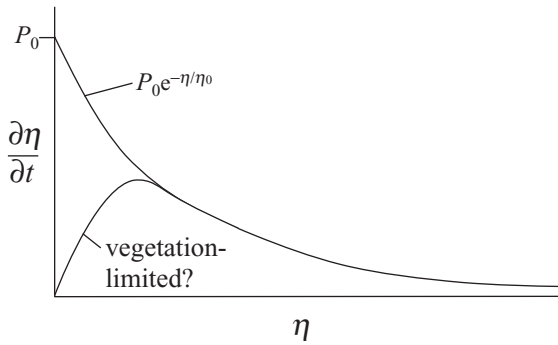


**Fig 1.5** Models for the relationship between regolith production and regolith thickness, illustrating the exponential model of Heimsath *et al.* (1997) and the alternative vegetation-limited model of Anderson and Humphrey (1990). The density contrast between the bedrock and sediment is assumed to be zero for simplicity.

arid-region hillslopes (Anderson and Humphrey, 1990; Strudley *et al.*, 2006). It should also be noted that the parameters  $P_0$  and  $\kappa$  may be approximately uniform along some hillslope profiles, but in general the hillslope and regolith-thickness profiles will influence the hillslope hydrology (e.g. the ratio of surface to subsurface flow), which will, in turn, modify the values of  $P_0$  and  $\kappa$  through time. Thinner regolith, for example, can be expected to increase surface runoff, thereby increasing  $\kappa$  and decreasing  $P_0$  in a positive feedback.

Equations (1.1) and (1.2) suggest that even in well-studied geomorphic systems such as hillslopes, quantifying the behavior of even the most basic elements is a significant challenge. This challenge provides an opportunity for mathematical modeling to play an essential role in geomorphic research, however, because most geomorphic systems are too complex to be fully understood and interpreted with field observations, measurements, and geochronologic techniques alone. The coupled hillslope evolution model of Eqs. (1.1) and (1.2) also illustrates a larger point: many geomorphic systems of greatest interest involve the coupling of different process domains (in this case the hillslope weathering and sediment transport regimes). Other key process-domain linkages occur at the juncture between the hillslope and the channel head, the

channel bed and channel bank, and the channel bed and shoreline, just to name a few.

The transition between the hillslope and fluvial channel system occurs where the shear stress of overland flow is sufficient to entrain hillslope material. In addition, the rate of sediment excavation from the channel head by overland flow must be greater than the rate of sediment infilling by creep and other hillslope processes. Empirically, this transition occurs where the product of the topographic gradient and the square root of contributing area is greater than a threshold value (Montgomery and Dietrich, 1999):

$$SA^{\frac{1}{2}} = X^{-1} \quad (1.5)$$

where  $S$  is the topographic gradient or slope,  $A$  is the contributing area, and  $X$  is the drainage density (i.e. equal to the ratio of the total length of all the channels in the basin to the basin area). The value of  $X$  depends on the texture and permeability of the regolith, hillslope vegetation type and density, and on the relative importance of different hillslope processes.

### 1.1.3 Bedrock channels

Channels are divided into alluvial and bedrock channel types depending on whether or not alluvium is stored on the channel bed. In bedrock channels, the transport capacity of the channel is greater than the upstream sediment flux. Sediment storage is rare or nonexistent in these cases. In alluvial channels, upstream sediment flux is greater than the transport capacity of the channel and alluvium fills the channel bed as a result. The distinction between bedrock and alluvial channels is important for understanding how they evolve. In order for bedrock channels to erode their beds they must pluck or abrade rock from the bed. Once rock material is eroded from a bedrock river it is usually transported far from the site of erosion because the flow velocity needed to transport material is typically much lower than the velocity required for plucking or abrasion. Bedrock channels erode their beds by a combination of plucking, abrasion, and cavitation. Plucking occurs when the pressure of fast-flowing water over the top of a jointed rock causes sufficient Bernoulli lift to dislodge rock from the bed. Abrasion occurs as saltating

bedload impacts the bed, chipping away small pieces of rock. Cavitation occurs when water boils under conditions of very high pressure and shear stress. Imploding bubbles in the water create pressures sufficient to pulverize the rock. Conditions conducive to cavitation are most likely to occur in rare large floods. The relative importance of plucking and abrasion depend primarily on lithology. Abrasion is generally considered to be the dominant process in massive bedrock lithologies such as granite (Whipple *et al.*, 2000). In sedimentary rocks, abrasion and plucking are both likely to be important.

Several mathematical models exist for modeling bedrock channel evolution. In the stream-power model, first proposed by Howard and Kerby (1983), the rate of increase or decrease in channel bed elevation is equal to the difference between the uplift rate and the erosion rate. The erosion rate is a power function of drainage area and channel-bed slope:

$$\frac{\partial h}{\partial t} = U - K_w A^m \left| \frac{\partial h}{\partial x} \right|^n \quad (1.6)$$

where  $h$  is the local elevation,  $t$  is time,  $U$  is uplift rate,  $K_w$  is a constant that depends on bedrock erodibility and climate,  $A$  is the drainage area,  $m$  and  $n$  are empirical constants, and  $x$  is the distance along the channel. The general form of the stream-power model also includes an additional constant term that represents a threshold shear stress for erosion (Whipple and Tucker, 1999). The stream-power model is empirically based: Howard and Kerby (1983) found that Eq. (1.6) successfully reproduced observed erosion rates at a site in Perth Amboy, New Jersey, measured by repeat survey. Their analysis cannot, however, rule out whether other variables correlated with drainage area and slope are the fundamental controlling variables of bedrock erosion. Nevertheless, the stream power is based on the physically-reasonable assumption that the erosive power of floods increases as a function of drainage area (which controls the volume of water routed through the channel) and channel-bed slope (which controls the velocity of that water for otherwise similar drainage areas and precipitation intensities). Calibrations of the stream-power model in natural systems suggest that

erosion is usually linear with slope (i.e.  $n \approx 1$  and  $m \approx 1/2$  (Kirby and Whipple, 2001)).

In steady state, uplift and erosion are in balance and  $\partial h/\partial t = 0$ . Equation (1.6) predicts that channel slope,  $S = |\partial h/\partial x|$ , is inversely proportional to a power-law function of drainage area,  $A$ , for drainage basins in topographic steady state:

$$S = \frac{U}{K_w} A^{-m/n} \quad (1.7)$$

Equation (1.7) predicts that, as drainage area increases downstream, the channel slope must decrease in order to maintain uniform erosion rates across the landscape. This inverse relationship between slope and area is responsible for the concave form of most bedrock channels.

Equation (1.7) can be used to derive an analytic expression for the steady-state bedrock channel longitudinal profile. To do this, we must relate the drainage area,  $A$ , to the distance along the channel from the channel head,  $x$ . The relationship between area and distance depends on the planform (i.e. map-view) shape of the basin. For a semi-circular basin, the square root of drainage area is proportional to the distance from the channel head. Adopting that assumption together with the empirical observation  $m/n = 0.5$ , Eq. (1.7) becomes

$$\frac{\partial h}{\partial x} = -\frac{C}{x} \quad (1.8)$$

where  $\partial h/\partial x$  has been substituted for  $S$  and  $C$  is a constant that combines the effects of uplift rate, bedrock erodibility, climate, and basin shape. Integrating Eq. (1.8) gives

$$h - h_0 = -C \ln\left(\frac{x}{L}\right) \quad (1.9)$$

where  $h_0$  is the elevation of the base of the channel at  $x = L$ . Figure 1.6 shows the longitudinal profile of the main channel of Hanaupah Canyon together with a plot of Eq. (1.9). The model fits the observed profile quite well using  $C = 0.9$  km.

The evolution of a hypothetical bedrock channel governed by the stream-power model is illustrated qualitatively in Figure 1.7a. A small reach of the channel's longitudinal profile is shown at times  $t_1$ ,  $t_2$ , and  $t_3$ . If the section is relatively small and has no major incoming tributaries, the drainage area can be considered uniform

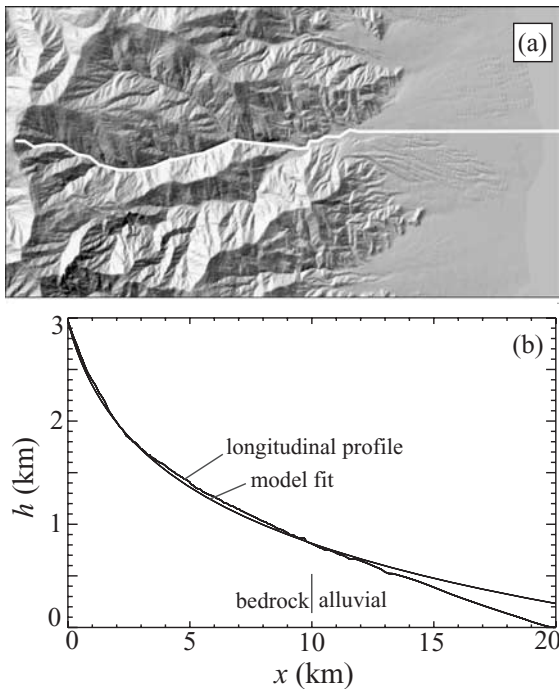


**Fig 1.6** (a) Shaded-relief image of the Hanaupah Canyon drainage network and alluvial fan. Location of longitudinal profile shown as white curve. (b) Longitudinal profile of main Hanaupah Canyon channel, together with best-fit to Eq. (1.8).

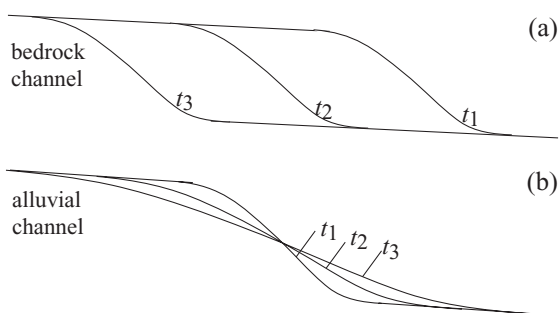


**Fig 1.7** Schematic diagrams of the evolution of (a) bedrock and (b) alluvial channels through time, illustrating the advective behavior of bedrock channels and the diffusive behavior of alluvial channels.

throughout the reach. If drainage area is uniform and  $n = 1$  is assumed, the erosion rate is proportional to the channel slope according to the stream-power model. Accordingly, steeper portions of the bed will erode faster, result-

ing in the propagation of knickpoints upstream as topographic waves. The rate of knickpoint propagation is equal to  $K_w A^m$ , i.e. knickpoints propagate faster in larger channels, wetter climates, and areas of more easily-eroded bedrock. The stream-power model will serve as the type example of the advection/wave equation studied in Chapter 4.

The Kern River (Figures 1.8 and 1.9) provides a nice example of knickpoint propagation in action. Two distinct topographic surfaces have long been recognized in the landscape of the southern Sierra Nevada (Webb, 1946) (Figure 1.8). The Boreal surface is a high-elevation, low-relief plateau that dips to the west at  $1^\circ$  (Figure 1.8b). The Chagoopa Plateau is an intermediate topographic “bench” that is restricted to the major river canyons and inset into the Boreal Plateau (Webb, 1946; Jones, 1987). Figure 1.8b maps the maximum extents of the Chagoopa and Boreal Plateaux based on elevation ranges of 1750–2250 m (Chagoopa) and 2250–3500 m a.s.l. (Boreal). Associated with each surface are prominent knickpoints along major rivers. Knickpoints along the North Fork Kern River, for example (Figure 1.9b), occur at elevations of 1600–2100 m and 2500–3300 m a.s.l. The stepped nature of the Sierra Nevada topography is generally considered to be the result of two pulses of Cenozoic and/or late Cretaceous uplift (Clark *et al.*, 2005; Pelletier, 2007c). According to this model, two major knickpoints were created during uplift, each initiating a wave of incision that is still propagating headward towards the range crest.

Recent work has highlighted the importance of abrasion in controlling bedrock channel evolution. In the abrasion process it is sediment, not water, that acts as the primary erosional agent. In the stream-power model, the erosive power is assumed to be a power function of drainage area. Although sediment flux increases with drainage area, upstream relief also plays an important role in controlling sediment flux. As such, the stream-power model does not adequately represent the abrasion process. Sklar and Dietrich (2001, 2004) developed a saltation-abrasion model to quantify this process of bedrock channel erosion. Insights into their model can be gained by replacing drainage area with sediment flux in the

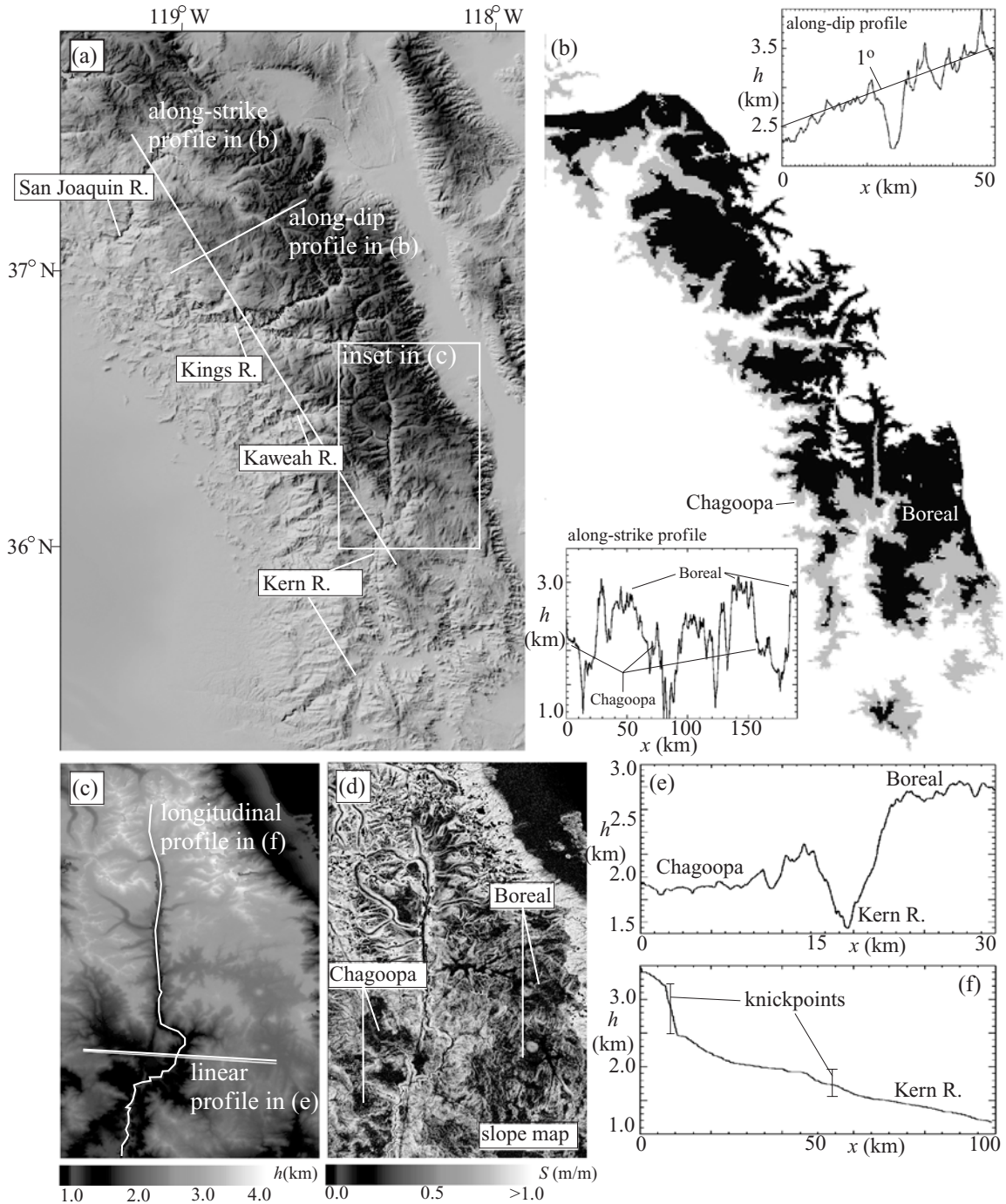


**Fig 1.8** Major geomorphic features of the southern Sierra Nevada. (a) Shaded relief map of topography indicating major rivers and locations of transects plotted in b. (b) Maximum extents of the Chagoopa and Boreal Plateaux based on elevation ranges of 1750–2250 m and 2250–3500 m a.s.l. Also shown are along-strike and along-dip topographic transects illustrating the three levels of the range in the along-strike profile (i.e. incised gorges, Chagoopa and Boreal Plateaux) and the westward tilt of the Boreal Plateau in the along-strike transect. (c) and (d) Grayscale map of topography (c) and slope (d) of the North Fork Kern River, illustrating the plateau surfaces (e) and their associated river knickpoints (f). For color version, see plate section. Modified from Pelletier (2007c). Reproduced with permission of Elsevier Limited.

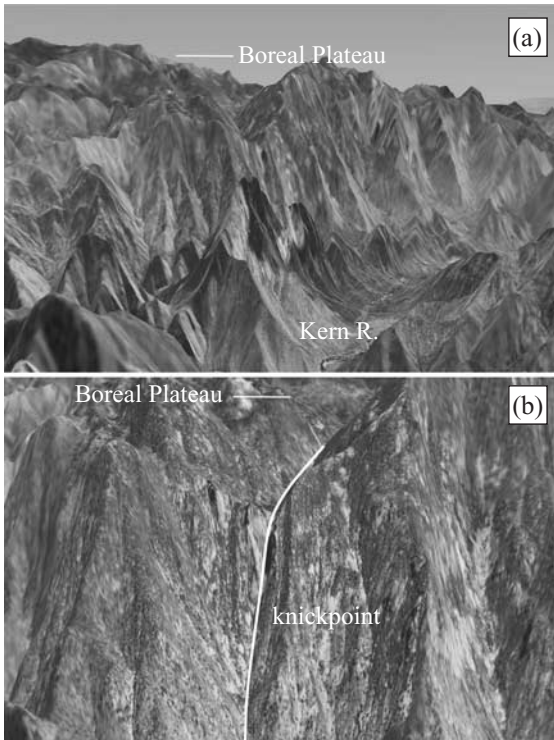


**Fig 1.9** Virtual oblique aerial photographs of portions of the Kern River basin. (a) The upper portion of the basin is characterized by the low-relief Boreal Plateau. The mainstem Kern River is incised 1–2 km into the Boreal Plateau. (b) Relief between the Boreal Plateau and Kern River is accommodated by a series of channel knickpoints along the Kern River and its tributaries.

stream-power model to obtain a sediment-flux-driven model:

$$\frac{\partial h}{\partial t} = U - K_s Q_s^m \left| \frac{\partial h}{\partial x} \right|^n \quad (1.10)$$

where  $Q_s$  is the sediment flux and  $K_s$  is a new coefficient of erodibility.

The predictions of the stream-power and sediment-flux-driven models are similar for cases of uniformly uplifted, steady-state mountain belts. In such cases, erosion is spatially uniform (everywhere balancing uplift) and therefore sediment flux  $Q_s$  is proportional to drainage area  $A$ . The predictions of the two models are very different, however, following the uplift of an initially low-relief plateau. In such cases, the stream-power model predicts a relatively rapid response to uplift because large rivers with sub-

stantial stream power drain the plateau. In the sediment-flux-driven model, however, low erosion rates on the plateau limit the supply of sediment that acts as cutting tools to channels draining the plateau edge. As a result, the sediment-flux-driven model leads to much slower rates of knick-point retreat than those predicted by the stream-power model in a plateau-type landscape (Gasparini *et al.*, 2006).

The sediment-flux-driven model also implies that the evolution of hillslopes and channels is more intimately linked than the stream-power model would suggest. In the stream-power model, hillslope evolution plays no explicit role in bedrock channel evolution. In the sediment-flux-driven model, however, increased hillslope erosion will supply more cutting tools to bedrock channels downstream. Downstream channels will respond to this increased supply with faster incision, further lowering the base level for hillslopes in a positive feedback. These ideas will be further explored in Chapter 4 where the stream-power and sediment-flux-driven models are compared in detail.

As one travels through the fluvial system, the transport capacity of the main channel generally increases with downstream distance as a result of increasing contributing area. The effect of declining channel slope, however, partially offsets that effect. As a result, transport capacity increases downstream, but not as rapidly as the sediment supply that the channel is required to transport. The bedrock-alluvial transition occurs where the sediment supply exceeds the transport capacity. In most drainage basins of the western US, the bedrock-alluvial transition occurs upstream of the mountain front (e.g. Figure 1.10). Only in regions that are tectonically most active does the bedrock-alluvial transition occur at the mountain front itself.

#### 1.1.4 Alluvial channels

Alluvial channels evolve in a fundamentally different style than that of bedrock channels (Figure 1.7). Alluvial channel evolution is governed by a conservation of mass relationship which states that the change in channel-bed elevation is equal to the gradient in bedload sediment flux along

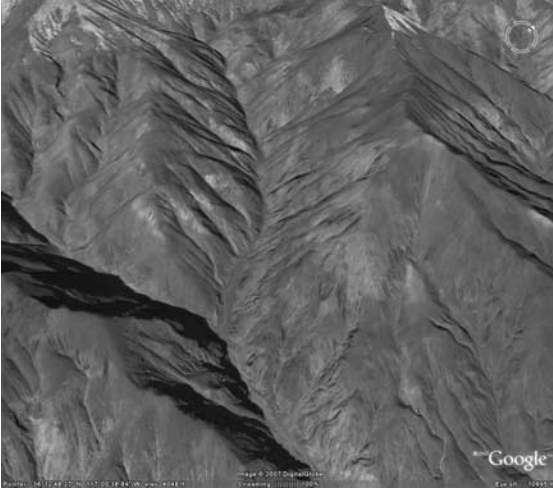


**Fig 1.10** Oblique perspective image of channels of Hanaupah Canyon. Smaller channels carve directly into bedrock, while the largest channels have wider beds filled with alluvium. Reproduced with permission of DigitalGlobe.

the channel profile:

$$\frac{\partial h}{\partial t} = -\frac{1}{c_0} \frac{\partial(wq_s)}{\partial x} \tag{1.11}$$

where  $h$  is the elevation of the channel bed,  $t$  is time,  $c_0$  is the volumetric concentration of bed sediment,  $w$  is the channel width,  $q_s$  is the sediment discharge per unit channel width, and  $x$  is the distance downstream. Equation (1.11) is simply a statement of conservation of mass, i.e. the channel bed must aggrade if the sediment-flux gradient is negative (if more sediment enters the reach from upstream than leaves it downstream) and incise if the sediment-flux gradient is positive (if more sediment leaves the reach than enters it). A number of different relationships exist for quantifying bedload sediment flux in alluvial channels, but one common approach quantifies sediment discharge as a linear function of channel gradient and a nonlinear function of the discharge per unit channel width:

$$q_s = -B \left( \frac{Q}{w} \right)^b \frac{\partial h}{\partial x} \tag{1.12}$$

where  $B$  is a mobility parameter related to grain size,  $Q$  is water discharge, and  $b$  is a constant. The value of  $b$  is constrained by sediment rating curves and is generally between 2 and 3 for bed-

load transport. If channel width is assumed to be uniform along the longitudinal profile, the combination of Eqs. (1.11) and (1.12) gives the classic diffusion equation (Begin *et al.*, 1981):

$$\frac{\partial h}{\partial t} = \kappa \frac{\partial^2 h}{\partial x^2} \tag{1.13}$$

where the diffusivity is given by  $\kappa = (BQ^b)/(c_0 w_0)$ , and  $w_0$  is the uniform channel width. The diffusive evolution of alluvial channels of uniform width is illustrated schematically in Figure 1.7b.

### 1.1.5 Alluvial fans

Deposition occurs on alluvial fans primarily because of channel widening near the mountain front. Abrupt widening decreases the transport capacity with distance downfan. Under such conditions, Eq. (1.11) predicts aggradation and fan development.

Hanaupah Canyon has one of the most spectacular alluvial fans in the western US. The size of the Hanaupah Canyon fan reflects the large sediment flux draining from Hanaupah Canyon, which, in turn, is a result of the high relief and semi-arid climate of this drainage basin. The semi-arid climate maximizes runoff intensity while minimizing erosion-suppressing vegetation cover. Many alluvial fans in the western US, including Hanaupah Canyon fan, have a series of distinct terraces (Figure 1.11) that rise like a flight of stairs from the active channel, with older terraces occurring at higher topographic positions relative to the active channel. Alluvial-fan terraces in many areas of the western US can be correlated on the basis of their elevation above the active channel, their degree of desert pavement and varnish development, and their extent of degradation. Terraces form as a result of changes in the ratio of sediment supply to transport capacity through time. During times when the ratio of sediment supply to transport capacity is high, aggradation and channel widening operate in a positive feedback that grows the fan vertically and radially. During times when the ratio of sediment supply to transport capacity is low, incision and channel narrowing operate in a positive feedback that causes the channel to entrench into older fan deposits, leaving an abandoned terrace.

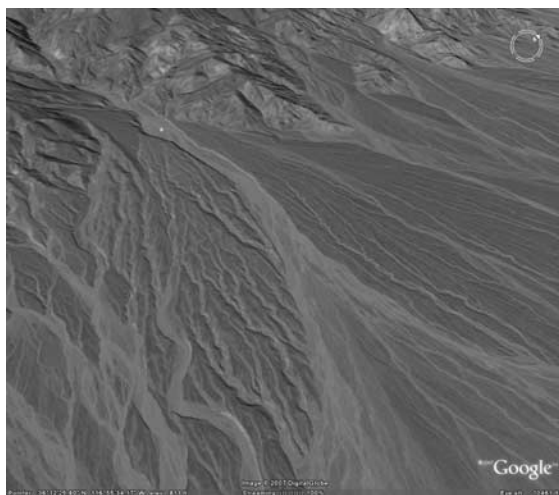


**Fig 1.11** Oblique perspective image of the terraces of Hanaupah Canyon fan. Reproduced with permission of DigitalGlobe. Younger terraces are lighter in color in this image, representing the relatively limited time available for desert pavement and varnish formation on younger surfaces.

Over time, episodes of aggradation, incision, and lateral reworking produce a nested sequence of terraces.

Multiple cut and fill cycles on alluvial fans create a spatially-complex, distributary channel network that presents a challenge to floodplain managers in the western US. The Tortolita Mountains fan northwest of Tucson, Arizona is a classic example. Figure 1.12 presents four views of this topographic complexity using a shaded relief image, aerial photo, grayscale map of a numerical model of flow depth during a recent extreme flood, and a surficial geologic map. The surficial geologic map (Figure 1.12d) was constructed by integrating soil development and other indicators of terrace age to group the terraces into distinct age ranges (Gile *et al.*, 1981; McFadden *et al.*, 1989). The surface age represents the approximate time since deep flooding occurred on the terrace because soils would be stripped from a terrace subjected to deep scour and buried on a surface subjected to significant fluvial deposition. Surficial geologic mapping indicates that flood risk (which is inversely correlated with surface age) varies greatly even at scales less than 1 km. The modeled flow depths also illustrate the spatial complexity of flooding. As Figure 1.12c, the

main channels on the fan branch into dozens of distributary channels separated by horizontal distances of only a few hundred meters or less.

The triggering mechanisms for alluvial-fan terrace formation have long been debated, but climatic changes most likely play a significant role in controlling the changes in sediment supply that trigger fan aggradation and incision. A growing database of surface and stratigraphic age estimates suggests that Quaternary geomorphic surfaces and underlying deposits of the western US can be correlated regionally (Christensen and Purcell, 1983; Bull, 1991; Reheis *et al.*, 1996; Bull, 1996). Several studies have documented fill events and/or surface exposure dates between 700–500 ka, 150–120 ka, 70–50 ka, and 15–10 ka corresponding to the Q2a, Q2b, Q2c, and Q3 geomorphic surfaces identified by Bull (1991) (surface exposure ages correspond to youngest ages in these ranges). Similarity of ages regionally has provided preliminary support for the hypothesis that Quaternary alluvial-fan terraces are generated by climatic changes.

Changes in sediment supply due to climatic changes can result from several factors, but variations in drainage density are likely to play a significant role in controlling the temporal variations in sediment flux from drainage basins in the western US. Terrace formation during the Pleistocene–Holocene transition is associated with a ten-fold increase in sediment supply (e.g. Weldon, 1980). It is unlikely that a change in precipitation alone could account for such large increases in sediment supply. During Pleistocene climates, vegetation densities were higher at most elevations across the western US. Higher vegetation density results in a lower drainage density. During times of lower drainage density, accommodation space is created in hollows for the deposition of sediment eroded from higher up on the hillslope, thereby lowering sediment fluxes from the basin relative to long-term geologic averages. During humid-to-arid transitions, drainage densities increase, removing sediment stored as colluvium in hollows during the previous humid interval. Sediment fluxes decrease when the drainage density reaches a new maximum in equilibrium with the drier climate. According to this model, it is the *change* in climate,